Pressure-induced magnetic transition in metallic nickel hydrides by *ab initio* pseudopotential plane-wave calculations

Xiaojiao San, Yanming Ma, Tian Cui,* Wenjiong He, Bai Han, Bingbing Liu, and Guangtian Zou
National Laboratory of Superhard Materials, Jilin University, Changchun 130012, People's Republic of China
(Received 11 November 2005; revised manuscript received 17 July 2006; published 24 August 2006)

The effects of pressure on the nickel hydrides NiH_x with different hydrogen concentrations (x=0, 0.25, 0.375, 0.5, 0.625, 0.6875, 0.75, and 1) have been extensively studied using the *ab initio* pseudopotential plane-wave method. A pressure-induced ferromagnetic (FM) to paramagnetic (PM) phase transition has been predicted. The hydrogen concentration-pressure phase diagram up to several megabar has been obtained. The transition pressure from FM to PM decreases with increasing hydrogen concentration. It is found that the electron transfers from 4*p* and 4*s* to 3*d* inside each Ni atom and from 4*p* and 4*s* of Ni atoms to H 1*s* are the main causes of the hydrogen-doping induced magnetic transition, while the electron transfers from the nearest-neighbor Ni 4*p* to H 1*s*, the nearest-neighbor Ni 4*p* to the further Ni 4*s*, and from 4*p* to 4*s* and 3*d* inside each Ni atom mainly contribute to the pressure-induced magnetic transition.

DOI: 10.1103/PhysRevB.74.052405 PACS number(s): 62.50.+p, 71.20.−b, 75.30.Kz

Metal-hydrogen systems have attracted much attention due to their importance in basic research and technological applications, such as a fuel storage mechanism for supereffective electrochemical cells, as a catalyst, etc. Some of the bulk properties of metals may be significantly changed due to the addition of hydrogen, such as the degradation of mechanical properties,[1] the modification of superconducting properties,[2–4] and the transition of magnetic properties.[5]

In the case of nickel-hydrogen systems, many investigations have concentrated on the storage of hydrogen in nanocrystalline nickel, nickel-base alloy, and a large-cluster-nickel surface[6–9] concerning the hydrogen behavior of transport, permeation, and absorption, etc. Besides that, there are many reports on nickel hydrides[5,10–12] and on vacancy in nickel hydrides[13] at normal pressure. In experiment, Bauer and Schmidibauer[5] observed that the introduction of hydrogen induced a ferromagnetic (FM) to paramagnetic (PM) phase transition in nickel hydrides (NiH_x) when the H concentration x was up to 65%. Vargas and Christensen[10] calculated the band structure of NiH_x (x=0,0.25,0.5,0.75,1.0) based on the linear-muffin-tin-orbital (LMTO) formalism with the local-density approximation for the exchange and correlation functional. Their results indicated a magnetic transition in NiH_x

With the advance in diamond anvil cell technology and x-ray diffraction techniques, many new phase transitions in solids under megabar pressures have been detected.[14–19] As for the effect of pressure on Ni, it was suggested that the fcc structure of nickel was stable up to 65 GPa at room temperature.[20] McMahan and Albers[21] gave a prediction that Ni would transform to an insulator at 34 TPa and revert back to a metal at 51 TPa, based on the self-consistent augmented-plane-wave (APW) calculations. Roy[22] suggested that there might be a pressure-induced ferromagnetism (FM) to paramagnetism (PM) phase transition in nickel. However, the pressure effect on the nickel hydrides is still less reported. In this Brief Report, the effects of H concentration and pressure on the magnetic properties in NiH_x are extensively studied using the *ab initio* method. A pressure-induced FM to PM phase transition in nickel-hydrogen systems is predicted. The transition pressure reduces with the increase of hydrogen concentration. The electron transfers with pressure from 4*p* to 4*s* and 3*d* inside Ni atom, from the nearest-neighbor Ni 4*p* to H 1*s*, and further Ni 4*s* are attributed to the magnetic phase transition.

Pseudopotential plane-wave *ab initio* calculations[23] are performed within the framework of density-functional theory through the CASTEP code.[24] The general gradient approximation[25] exchange-correlation functional is employed. An ultrasoft pseudopotential is generated with an atomic electronic configuration of $3d^8 4s^{1.27} 4p^{0.73}$ for Ni and $1s^1$ for H, respectively. Geometries under pressures are optimized for Ni from fcc, bcc, hcp, and bct structures,[26,27] for NiH from NaCl, wurtzite, CsCl, NiAs, blende-type structures,[28] and for $NiH_{0.5}$ from some candidate structures constructed from NiH with wurtzite, NiAs, and blende structures by deleting a hydrogen atom (denoted as wurtzite-I, NiAs-I, and blende-I hereafter), and from Ni with bcc and fcc structures by adding a hydrogen atom (denoted bcc-I and fcc-I), respectively. The equations of state (EOSs) for all structures are shown in Fig. 1. The results indicate that within our investigated pressures, the stable sites for hydrogen atoms in Ni are the interstitial sites in a fcc Ni crystal lattice with octahedral symmetry. Two $2\times1\times1$ supercells constructed with the unit cell of $NiH_{0.5}$ and $NiH_{0.75}$ are used to realize the Ni hydrides with H concentrations of 0.375 and 0.625, respectively. One of the $2\times2\times1$ supercells was constructed with $NiH_{0.75}$ to realize the H concentration of 0.6875. A convergence test to give an energy cutoff of 330 eV for all NiH_x (x=0.0–1.0) and a $16\times16\times16$ Monkhost pack grid is used in the electronic Brillouin zone integration for all structures with the exception of $NiH_{0.375}$ and $NiH_{0.625}$ with an $8\times12\times12$ grid and $NiH_{0.6875}$ with an $8\times8\times12$ grid. All the calculations performed here are spin-polarized.

The theoretical lattice constants in NiH_x (x=0,0.25,0.5,0.75,1.0) at zero pressure, together with the tight-binding calculations,[29] the LMTO results,[10] and the experimental measurement,[30] are listed in Table I. Our PW calculations in the equilibrium lattice constant and bulk modu-

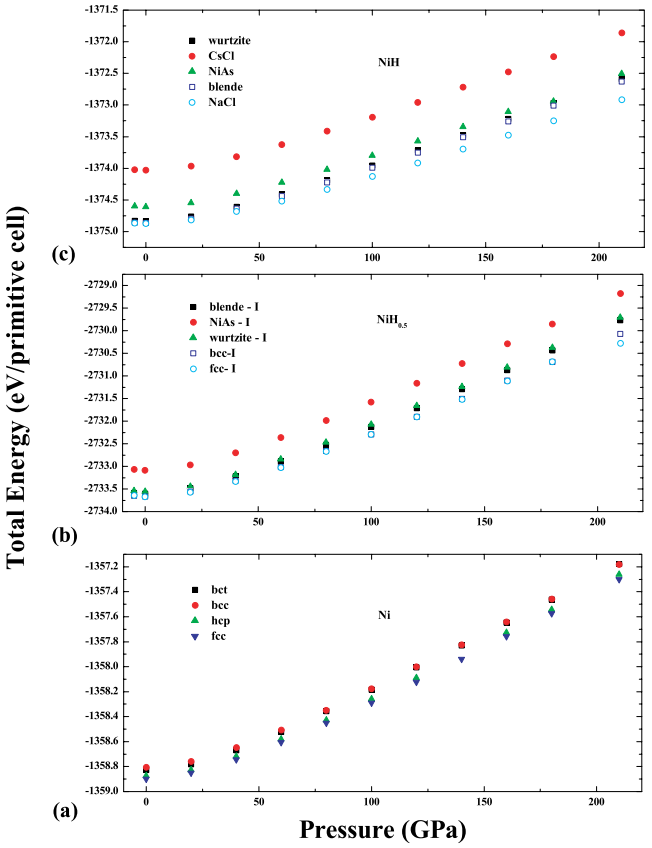

FIG. 1. (Color online) Calculated total energies for Ni (a), $NiH_{0.5}$ (b), and NiH (c) in various crystal structures as a function of pressure.

lus for nickel and nickel hydrides are in excellent agreement with the experimental measurement. The bulk modulus of NiH_x shown in Table I decreases with the H concentration up to $x=0.25$, and then increases with larger x. The density of states (DOS) at the Fermi level $[N(E_F)]$ for NiH_x is also listed in Table I. It is found that $N(E_F)$ increases with H concentration, and then decreases as $x>0.25$. This fact in $N(E_F)$ may contribute to the anomalous behaviors in the bulk modulus of NiH_x. The EOSs shown in Fig. 1 and the optimized structures for Ni and Ni hydrides suggest that the

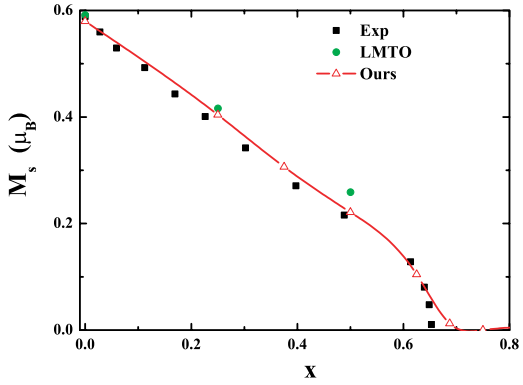

FIG. 2. (Color online) The saturation magnetization in NiH_x at zero pressure. The black squares represent the experimental curve (Ref. 5). The green circles represent the LMTO calculation (Ref. 10). The red hollow triangles represent our pseudopotential PW results.

stable sites for hydrogen atoms in Ni are the interstitial sites in a fcc Ni crystal lattice with octahedral symmetry without any obvious structural phase transitions induced by pressure in the pressure range from 0 to 210 GPa. This result agrees with the fact that in pure Ni there is no phase transition in experimental measurement up to 100 GPa,[31] and the theoretical prediction by McMahan *et al.*[21] up to 34 TPa, respectively.

It is known that the ferromagnetic properties of bulk Ni are sensitive to the presence of interstitial H atoms.[10] In this work, we examine the variations of magnetic properties of NiH_x with H concentration. Figure 2 shows the comparison of the calculated saturation magnetization with the experimental data[9] and previous LMTO (Ref. 10) calculations for NiH_x. It is clear that our calculations are in excellent agreement with the experimental results. The calculated saturation magnetization for NiH_x decreases with the increasing x as plotted in Fig. 2. Particularly, as H concentration x is up to 0.625, the saturation magnetization decreases steeply. The calculated saturation magnetization for $NiH_{0.75}$ and NiH equals zero, indicating a paramagnetic state in these two compounds. The addition of H atoms suppresses the ferromagnetism of pure Ni. For transition metals, theoretical and experimental research has confirmed that the magnetic prop-

TABLE I. The equilibrium lattice constants (in Å), bulk modulus (B_0 in GPa), and density of states at Fermi level $[N(E_F)$ in states $eV^{-1}]$ for NiH_x at zero pressure, including the tight-binding calculations (TB) (Ref. 29), the linear-muffin-tin-orbital (LMTO) (Ref. 10) results, the experimental measurement (Expt.) (Refs. 10 and 30), and our pseudopotential PW calculations.

H concentration x	a (Å)			B_0 (GPa)				$N(E_F)$ (eV^{-1})
	PW	TB[a]	LMTO[b]	Expt.[b]	PW	TB[a]	Expt.[c]	PW
0.00	3.54	3.43	3.51	3.52	191.1	268	186	7.89
0.25	3.60		3.53	3.59	183.1			9.24
0.50	3.66		3.65	3.66	185.6			8.91
0.75	3.70		3.74	3.72	186.8			8.83
1	3.75		3.74	3.72	188.3			4.22

[a]Reference 29.
[b]Reference 10.
[c]Reference 30.

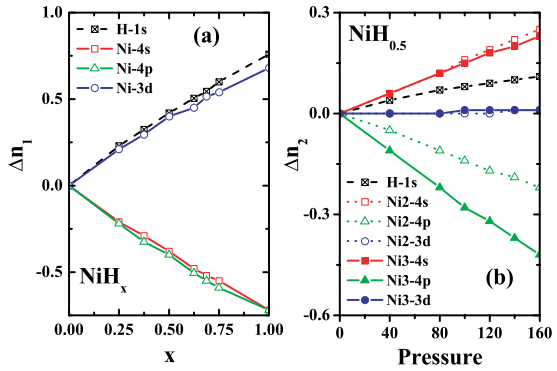

FIG. 3. (Color online) (a) The electron population for Ni 3*d*, 4*p*, 4*s*, and H 1*s* in NiH_x relatives to its atomic electronic configuration. (b) The electron population for Ni 3*d*, 4*p*, 4*s*, and H 1*s* in $NiH_{0.5}$ under different pressures relative to those at zero pressure (including the nearest-neighbor Ni-3 atom and the second-nearest-neighbor Ni-2 atom). The dashed, dotted, and solid lines represent H, Ni-2, and Ni-3, respectively. The black crossed squares, red squares, green triangles, and blue circles represent the H 1*s*, Ni 4*s*, Ni 4*p*, and Ni 3*d* electrons, respectively. *S* for the charge spilling parameter is around 2×10^{-3} under all the investigated pressures.

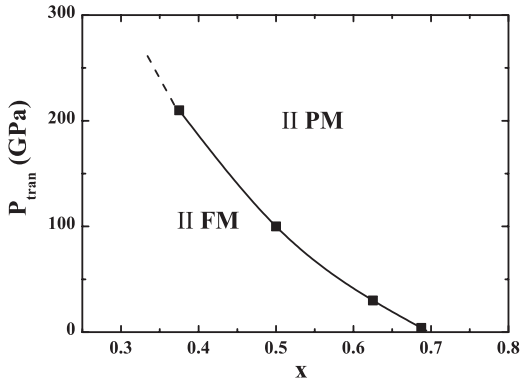

FIG. 4. The phase diagram of pressure vs H concentration in NiH_x. Phase I is the ferromagnetic state, while phase II is the paramagnetic state.

erties depend directly on the conduction electrons, including *s* and *d* electrons.[32] Using Mulliken population analysis,[33,34] the effect of H concentration on the electron population for Ni 3*d*, 4*p*, 4*s*, and H 1*s* in NiH_x related to its atomic electronic configuration has been shown in Fig. 3(a). It is clear that there exist electron transfers from 4*p* and 4*s* to 3*d* inside each Ni atom and from 4*p* and 4*s* of Ni atoms to H 1*s* due to the hybridization of the Ni 3*d* orbital with Ni 4*s* and Ni 4*p* orbitals, and the hybridization of the H 1*s* orbital with Ni 4*p* and Ni 4*s* orbitals. The fact that H doping influences the electron configuration of Ni and H itself acts as an acceptor result in the magnetic transition from FM to PM in NiH_x.

The net spin DOS represents the difference between contributions from majority- and minority-spin eigenstates, and a field for the net spin DOS can visualize the spatial distribution of the magnetic moment. Therefore, the magnetic information can be obtained from the net spin DOS. At zero pressure, the net spin DOS of $NiH_{0.5}$ shows strong structural features, while the intensities of the net spin DOS curve decrease with pressure. Up to 100 GPa, the net spin DOS vanishes, signaling a pressure-induced FM to PM transition happening in this compound. We also explored the spin-polarized band structure in $NiH_{0.5}$ with pressure. At zero pressure, the calculated band structure shows a strong splitting between the majority- and minority-spin bands. But the band splitting decreases with increasing pressure. When the pressure reaches 100 GPa, the band splitting totally vanishes. Thus, the band-structure calculations lend strong support to the observation of FM to PM transition in the net spin DOS.

The predicted FM to PM transition pressures for $NiH_{0.375}$, $NiH_{0.625}$, and $NiH_{0.6875}$ are 210, 30, and 4 GPa, respectively. Within the pressure range of 0–210 GPa, Ni and $NiH_{0.25}$ systems remain ferromagnetic, while $NiH_{0.75}$ and NiH compounds stay in a paramagnetic state. Thus, we conclude that the transition pressure decreases with H concentration. The phase diagram of pressure versus H concentration in NiH_x has been plotted in Fig. 4. The transition pressure has a continuous reduction with H concentration. In particular, the extrapolated critical value of *x* corresponding to zero transition pressure in Fig. 4 is ~0.7, which is in reasonable agreement with the experimental result of $x=0.65$.[9]

For understanding the physical origin of the pressure-induced FM to PM transition, we list the calculated charge (*Q*) and magnetic moment (*m*) for three atoms (one H atom and two Ni atoms) in the primitive cell of $NiH_{0.5}$ under different pressures in Table II, using Mulliken population analysis. Here we label the hydrogen atom as H-7, the second-nearest-neighbor nickel atom to hydrogen as Ni-2, and the nearest-neighbor one as Ni-3, the same as in Ref. 10. One notices that the magnetic moments for the two Ni atoms decrease with increasing pressure, in agreement with our previous prediction. At zero pressure, the magnetic moment of

TABLE II. The charge $Q(e)$ and magnetic moment $m(\mu_B)$ for two Ni atoms (Ni-2 and Ni-3) and one H atom (H-7) in the primitive cell of $NiH_{0.5}$ under different pressures. Ni-2 and Ni-3 represent the second-nearest-neighbor Ni atom to H atom and the nearest-neighbor one, respectively. The charge spilling parameter (*S*) for majority- and minority-spin components is around 2×10^{-3} under all the investigated pressures.

$NiH_{0.5}$ atom	0 GPa		40 GPa		80 GPa		100 GPa		120 GPa	
	Q	*m*	*Q*	*m*	*Q*	*m*	*Q*	*m*	*Q*	*m*
H-7	−0.21	0.00	−0.25	0.00	−0.28	0.00	−0.29	0.00	−0.30	0.00
Ni-2	0.08	0.40	0.07	0.29	0.06	0.15	0.05	0.00	0.04	0.00
Ni-3	0.13	0.15	0.18	0.10	0.22	0.06	0.24	0.00	0.26	0.00

Ni-2 is $0.40\mu_B$, larger than the value of $0.15\mu_B$ for Ni-3. Therefore, the farther the Ni atoms are away from the H atoms, the larger their magnetic moments are, while the magnetic moment contributed by H atoms is almost negligible. From Table II, at zero pressure, the charge of Ni-2 is 0.08e, while it is 0.13e for Ni-3. This indicates that the H atom mainly accepts charges from the nearest-neighbor Ni atom. As pressure increases, the charge for Ni-2 decreases and that for Ni-3 increases, while the total charge transfer from Ni atoms to H atom increases and the magnetic moment of all the Ni atoms decreases. The charge transfer from Ni-3 atom to H atom as well as to Ni-2 reduces the number of unpaired electrons of all the Ni atoms.

We show the pressure effects on the changes of the electron population of s, p, and d in $NiH_{0.5}$ in Fig. 3(b). There are three kinds of electron transfers among the atoms in the primitive cell, including from $4p$ to $4s$ and $3d$ inside each Ni atom, from Ni-3 $4p$ to H $1s$ between the nearest-neighbor Ni atom and hydrogen atom, and from Ni-3 $4p$ to Ni-2 $4s$ between the two Ni atoms with increasing pressure. The electron transfer tends to cause makes the minority- and majority-spin electrons to be balanced once the minority- and majority-spin electrons in Ni $3d$, $4s$, $4p$, states and H $1s$ state, respectively, can be counteracted; the magnetic moments disappear. Thus, the above electron transfer is responsible for the predicted FM to PM transition. Note that all the population curves with pressure show a weak discontinuity around 100 GPa. This weak discontinuity might be related to the observed transition at this pressure.

The above fact might be attributed to the screening of protons in jellium.[35,36] The H atom mainly forces the neighboring Ni atoms to supply charges and tends to cause the majority- and minority-spin electrons to be balanced. The screening length decreases and the screening effect increases with pressure, which enhances the interaction between two Ni atoms, so the charge transfer between the inequivalent Ni atoms occurs. As suggested in Fig. 3(b) and Table II, the electron transfers from the nearest-neighbor Ni $4p$ to H $1s$ and the second-nearest-neighbor Ni $4s$ increase with increasing pressure.

In summary, we have investigated the effect of pressure and H concentration on nickel hydrides using the *ab initio* pseudopotential plane-wave method. In the pressure range from 0 to 210 GPa, no obvious structural phase transition is observed in all the studied Ni-H systems. A pressure-induced FM to PM phase transition has been found. A hydrogen concentration-pressure phase diagram up to several megabar has been obtained. Most importantly, the transition pressure from FM to PM reduces with increasing H concentration. We have shown that the hydrogen-doping induced magnetic transition is caused by the electron transfers from $4p$ and $4s$ to $3d$ inside the Ni atom and from $4p$ and $4s$ of Ni atoms to H $1s$, while the pressure-induced magnetic transition is mainly attributed to the electron transfers from the nearest-neighbor Ni $4p$ to H $1s$, from the nearest-neighbor Ni $4p$ to the further Ni $4s$, and from $4p$ to $4s$ and $3d$ inside each Ni atom.

This work was supported by the NSAF of China, Grant No. 10276016, the National Natural Science Foundation of China under Grants No. 10574053, No. 10444001, and No. 10204010, 2004 NCET and 2003 EYTP of MOE of China, and National Basic Research Program of China, Grants No. 2005CB724400 and No. 2001CB711201.

*Author to whom all correspondence should be addressed. Electronic address: cuitian@jlu.edu.cn

[1] S. M. Myers *et al.*, Rev. Mod. Phys. **64**, 559 (1992).
[2] B. Stritzker and H. Wühl, in *Hydrogen in Metals II*, edited by G. Alefeld and J. Völkl, Topics in Applied Physics Vol. 29 (Springer, Berlin, 1978), p. 243.
[3] B. Stritzker, Z. Phys. **268**, 261 (1974).
[4] A. M. Lamoise *et al.*, J. Phys. (France) Lett. **36**, L271 (1975).
[5] H. J. Bauer and E. Schmidibauer, Z. Phys. **164**, 367 (1961).
[6] C. Marte and R. Kirchhein, Scr. Mater. **37**, 1171 (1997).
[7] Omar A. El kebir and Andrzej Szummer, Int. J. Hydrogen Energy **27**, 793 (2002).
[8] Roi Baer *et al.*, Phys. Rev. B **55**, 10 952 (1997).
[9] Thomas H. Upton and William A. Goddard III, Phys. Rev. Lett. **42**, 472 (1979).
[10] P. Vargas and N. E. Christensen, Phys. Rev. B **35**, 1993 (1987).
[11] X. W. Lin *et al.*, Phys. Rev. Lett. **56**, 1835 (1986).
[12] H. Smithson *et al.*, Phys. Rev. B **66**, 144107 (2002).
[13] Changjun Zhang and Ali Alavi, J. Am. Chem. Soc. **127**, 9808 (2005).
[14] A. Jayaraman, Rev. Mod. Phys. **55**, 65 (1983).
[15] A. Jayaraman, Rev. Sci. Instrum. **57**, 1013 (1986).
[16] H. K. Mao *et al.*, Solid State Commun. **74**, 1027 (1990).
[17] Y. K. Vohra *et al.*, Science **231**, 1136 (1986).
[18] T. Palasyuk and M. Tkacz, Solid State Commun. **130**, 219 (2004).
[19] P. Vaqueiro *et al.*, Phys. Rev. B **63**, 064106 (2001).
[20] David A. Young, *Phase Diagrams of the Element* (University of California Press, Berkeley, 1991), p. 182.
[21] A. K. McMahan and R. C. Albers, Phys. Rev. Lett. **49**, 1198 (1982).
[22] R. Roy, in *Phase Transitions*, edited by H. K. Heinisch, R. Roy, and L. E. Cross (Pergamon Press, Oxford, 1973).
[23] David J. Singh, *Planewaves, Pseudopotentials and the LAPW Method* (Naval Research Laboratory, Washington, D.C., 1994).
[24] M. Segall *et al.*, J. Phys.: Condens. Matter **14**, 2717 (2002).
[25] J. P. Perdew *et al.*, Phys. Rev. Lett. **77**, 3865 (1996).
[26] E. G. Moroni *et al.*, Phys. Rev. B **56**, 15629 (1997).
[27] D. A. Papaconstantopoulos *et al.*, Phys. Rev. B **39**, 2526 (1989).
[28] H. Smithson *et al.*, Phys. Rev. B **66**, 144107 (2002).
[29] Michael J. Mehl and Dimitrios A. Papaconstantopoulos, Phys. Rev. B **54**, 4519 (1996).
[30] R. Gaudoin and W. M. C. Foulkes, Phys. Rev. B **66**, 052104 (2002).
[31] C. S. Yoo *et al.*, Phys. Rev. Lett. **84**, 4132 (2000).
[32] D. Feng, *Physics in Metals* (Scientific, Nanjing, 2000).
[33] M. D. Segall *et al.*, Mol. Phys. **89**, 571 (1996a).
[34] M. D. Segall *et al.*, Phys. Rev. B **54**, 16317 (1996b).
[35] C. O. Almbladh *et al.*, Phys. Rev. B **14**, 2250 (1976).
[36] J. Condzik and H. Stachowiak, J. Phys. C **18**, 5399 (1985).